Research Square

Preprints are preliminary reports that have not undergone peer review.
They should not be considered conclusive, used to inform clinical practice,
or referenced by the media as validated information.

Microbubble CO_2 Injection in High- Perm Sandstone: Flow-Rate Effects and Permeability Decay

Theo Le Gallais
t.legallais@postgrad.curtin.edu.au
Curtin University
Egi Adrian Pratama
Curtin University
Klaus Regenauer-Lieb
Curtin University
Mohammad Sarmadivaleh
Curtin University
Ali Saeedi
Curtin University
Quan Xie
Curtin University
Hideto Kurokawa
Tokyo Gas (Australia)

Research Article

Keywords: Geological CO_2 storage, Microbubble CO_2 injection, High-permeability sandstone, Sweep efficiency, Permeability decay

Posted Date: March 6th, 2026

DOI: https://doi.org/10.21203/rs.3.rs-8879243/v1

License: This work is licensed under a Creative Commons Attribution 4.0 International License. Read Full License

Additional Declarations: Competing interest reported. Theo Le Gallais reports that financial support was provided by Tokyo Gas Australia Pty Ltd. His tuition fees for PhD candidacy have been off-set by Curtin University.The other authors declare that they have no known competing financial interests or personal relationships that could have appeared to influence the work reported in this paper.

Abstract

Microbubble (MB) CO_2 injection has been proposed to improve sweep efficiency and dissolution trapping, yet its implications for injectivity and near-wellbore integrity in high-permeability formations are not well constrained. We conducted repeated volume-balance core-flooding experiments on high-permeability Berea sandstone (~ 980 mD) under deep saline aquifer conditions (40°C, 10.7 MPa), comparing MB and conventional supercritical CO_2 injections across flow rates of 0.05–0.5 cc/min (Ca : 1.15–11.5 × 10^{-9}) while monitoring brine permeability.

At 0.05 cc/min, MB injection increased average CO_2 saturation by 8.9% relative to conventional flooding due to temporary microbubble-induced blockage of dominant flow channels. This benefit diminished at higher flow rates (0.1–0.5 cc/min), where MB injection consistently yielded lower final CO_2 saturations. Across sequential floods, MB injection caused brine permeability to decline up to four times faster than conventional injection, indicating accelerated near-wellbore damage likely driven by fines mobilisation and enhanced mineral reactions associated with rapid microbubble dissolution.

These results demonstrate a clear trade-off in MB CO_2 injection: potential sweep-efficiency gains at low flow rates versus permeability loss and injectivity difficulties at higher flow rates. The results of this study suggest the need for further research under higher flow rates considering practical operation and optimising microbubble-based storage strategies will require careful control of flow rate and consideration of reservoir heterogeneity in high-permeability systems.

1. Introduction

Carbon dioxide is the principal emitted greenhouse gas responsible for unprecedented fast climate change. It is the co-product of every industry sector at the society's base and more globally, from every main source of energy used by mankind (IPCC, 2023). Moderating emissions is a current challenge that will persist in the next decades. Carbon capture, utilization and storage is considered a major actor in the transition to net-zero carbon by 2050 (IEA, 2020). Particularly, carbon storage is a major challenge in economic scales: Building a storage project includes many safety considerations with relative uncertainties (Mahjour & Faroughi, 2023).

Microbubble CO_2 is a new injection method that may be used in all storage settings. It has mainly been studied as displacing liquid for Enhanced Oil Recovery (EOR) (Xue et al., 2018). This technology benefits from a higher oil recovery by reducing entry capillary pressure (Li et al., 2024). By being able to penetrate smaller pores, CO_2 microbubble also implies a lower injectivity overall. Microbubbles can plug the main pathways, allowing flow through the smallest pores (Yu et al., 2022), resulting in a higher ΔP. This injection type has also been shown to be effective in aquifer settings as there is also potential for a more efficient storage. In these particular settings, microbubble injection has been mainly studied in a high salinity environment (Jiang et al., 2019; Park et al., 2018; Patmonoaji et al., 2019; Wang et al., 2022; Zhai et al., 2020). Overall, microbubble injection has a potential for a higher sweep efficiency, higher dissolution rate and a slower CO_2 plume rising velocity (Li et al., 2023).

The current state of the art in microbubble injection applied to laboratory-scale core flooding tests performed in deep saline aquifer conditions demonstrates a relative increase in average CO_2 saturation at the steady state. This improvement is attributed to the addition of a microbubble generation filter (Fig. 1). All values within sandstone rock samples never go above 20% increase in CO_2 saturation and on average 6.2%. Mainly Berea sandstone is used as test sample in literature floodings. Interestingly, it shows disparate results on the most

tested permeability: 100 mD. Samples done in rock cores show an average of 0 to 5% improvement thanks to microbubble injection.

Overall, a trend is showing up, where higher permeability samples have more potential to have better results with microbubble injection. This could be explained by the “Jamin effect”, detailed in publications (Dubey & Majumder, 2024; Le et al., 2022; Li et al., 2024; Telmadarreie et al., 2016). Jia et al. (2023) observed on microchips large channels plugged by microbubbles, which allowed smaller pores to be penetrated. A microbubble or a swarm of microbubbles with a larger diameter to the pore can block it and create a local higher pressure. CO_2 can then reach pores that required a higher capillary entry pressure to be swept. In the case of high-permeability sandstone samples, they possess high-diameter channels through which CO_2 can easily transit. Microbubble CO_2 agglomerates can temporarily plug them and allow other smaller channels to be penetrated.

From literature results, it can be noted that floodings on cores with a similar permeability may not obtain similar CO_2 saturation results. In fact, the relation between permeability and final CO_2 saturation after drainage is complex and no direct relation exists between them (Zhang & Arif, 2024). However, the microbubble effect on sweep efficiency and injectivity appears to depend on permeability, which can be seen from the correlation shown in Fig. 1. The effectiveness of microbubble injection can vary significantly, as the way microbubbles move through the rock may lead to inconsistent blockage; in addition, microbubbles of different sizes may interact with and block different pore spaces during each injection. Literature results also employed different salinities, ranging from 0.58 (Xue et al., 2013) to 187 g/L eqNaCl (Jiang et al., 2019; Patmonoaji et al., 2019; Zhai et al., 2020) which may have an impact on microbubble generation and flood.

The physical properties of microbubbles lead to improvements in sweep efficiency, injectivity and dissolution rate, as seen in the literature (Li et al., 2018; Park et al., 2018; Patmonoaji et al., 2019; Ueda et al., 2021; Wang et al., 2022; Xue, 2021; Xue & Matsuoka, 2008; Xue et al., 2014; Xue et al., 2018; Xue et al., 2011; Yu et al., 2022; Zhai et al., 2020). However, other effects of microbubbles could be considered and have the potential to antagonise the previously mentioned mechanisms. In near-wellbore environments, where the rock is exposed to high concentrations of CO_2 during injection, the fast dissolution of microbubbles can cause the surrounding brine to become acidic more quickly. This can accelerate the dissolution of minerals and chemical reactions within the pore spaces of the rock. Moreover, microbubbles negative charges on their boundaries could interact with clay particles and cause swelling. Overall, all these effects could cause fines migration and faster rock decay.

Most comparative laboratory tests have relied only on a single flowrate per experiment, which does not reflect real field conditions where the injection rate tends to be variable. Microbubble injection studies on a flowrate comparison point have noticed significant differences in results (Le et al., 2022; Wang et al., 2025b). In the case of Wang et al. (2025b), 0.05 cc/min on a standard syringe pump injection is seen as the most optimal case for microbubble injection. However, this injection flowrate on a closer reservoir is not to be expected but at least a hundred meters from the well in medium-sized projects. Economic viability is also unlikely if microbubbles must be generated at such a low rate, as it is insufficient for the field. Sequential flooding is used in this study to investigate microbubble injection rate sensitivity ; the effects on saturation and global microbubble behaviour are discussed.

This study investigates whether microbubble injection improves CO_2 saturation in high-permeability rocks, using CO_2 flooding experiments on Buffi Berea sandstone with a permeability of ~ 1000 mD. The flooding protocol of Zhai et al. (2020) was replicated at a flow rate of 0.05 cc/min on one sample (BO5). A second sample (BO3) was subjected to sequential CO_2 injections at increasing flow rates (0.05, 0.1, and 0.5 cc/min) to evaluate how changes in injection rate influence steady state saturations relative to conventional injection. The impact of microbubble injection on permeability reduction was investigated by monitoring brine permeability after the initial imbibition, for both conventional and microbubble injection, using sample BO3. To the best of our knowledge, this is the first study to systematically quantify flow-rate–dependent microbubble CO_2 behaviour and permeability decay in high-permeability sandstone under repeated injection cycles. By comparing microbubble and conventional CO_2 injection across sequential flow rates, we capture both efficiency gains and integrity losses. The findings provide insight directly relevant to CO_2 subsurface utilisation and geological storage operations.

2. Materials and Methods

Volume balance core flooding is a technique that measures the water volume output from the sample at all times during the CO_2 injection experiment. By subtracting the volume contained in the tubing (dead volume), the sample's global CO_2 saturation can be estimated. CO_2 saturation calculation from volume change is detailed:

$$S_g = \frac{V_{observed} - V_{dead\ volume}}{V_{pore}} * 100\ (\%)$$

$$S_g :\ CO_2\ gas\ saturation\ (\%)$$

$$V_{observed} : Observed\ water\ volume\ in\ cylinder\ (ml)$$

$$V_{dead\ volume} : Dead\ volume\ (ml)$$

$$V_{pore} : Connected\ pore\ volume\ in\ Core\ (supposed\ 100\%\ filled\ with\ brine\ after\ saturation)\ (ml)$$

Dead volume was measured previous to the flooding. The core holder is empty, and sleeves are connected directly. Water was injected until the tubing becomes full. Air is then injected to chase the water and recover the corresponding volume. This process has been done 20 times to ensure consistency of the dead volume. Experiments volumes are corrected by the dead volume, and the time is corrected to match zero when the dead volume has been reached.

Dead volume and cylinder measurements uncertainties resulted in an absolute uncertainty of 1.39% to 5% in CO_2 saturation depending on the used setup layout at the time of the experiment. It is mainly dependent on the standard deviation obtained through dead volume measurements (Table 1). Cylinder readings also introduce a volume measurement error of ± 0.25 ml. For microbubble tests, the filter pore volume was not sufficient to notice a significant dead volume measurement change. Therefore, similar dead volume measurements have been taken for both injection types. In all shown experiments, the mean value and standard deviation have been taken as the output results of a given setting.

Table 1
Absolute uncertainty associated with dead volume and measuring cylinder.

Test number	Absolute uncertainty (%CO_2)
1–2	1.91
3–13	2.01
14–28	4.98
29–33	1.39

These absolute uncertainties are expected to be found on the measured dataset; they are averaged to compute an expected variance and compared to the measured data.

Upon discharge from the back-pressure regulator, the brine undergoes two competing volumetric effects: expansion associated with pressure release and contraction associated with cooling. Upper-bound estimates of these effects were evaluated. Isothermal decompression of a 12.5 wt% NaCl brine from 10 MPa to 0.1 MPa at 40°C results in a volumetric expansion of approximately + 0.36%, based on an isothermal compressibility of 3.64 × 10^{-10} Pa^{-1}. The concurrent cooling of the brine from 40°C to 25°C produces a volumetric contraction of approximately − 0.6%, using an average volumetric thermal expansivity of 4.085 × 10^{-4} K^{-1} over this temperature interval. Values for brine compressibility and thermal expansivity were taken from Rogers and Pitzer (1982).

The combined effect of decompression and cooling therefore corresponds to a net volumetric decrease of approximately 0.24%, equivalent to 0.048 mL for a nominal volume of 20 mL, representing the maximum recoverable volume. This correction is significantly smaller than the uncertainty associated with dead-volume estimation and volumetric cylinder readings. Consequently, no correction for pressure- and temperature-induced volume changes was applied to the measurements.

2.1. Experimental apparatus

Core floodings setups are shown in Fig. 2. A Vinci double syringe pump was providing injection pressure. ISCO pumps were guaranteeing back pressure (260D) and confining pressure (500D). The setup temperature is guaranteed through a circulation model, where temperature is guaranteed by a circulating confining fluid, heated at an accumulator and moving thanks to a circulation pump (Eldex 1021 bb-4-2). Volume measurements are made from a 0.25ml precision water cylinder. Supercritical CO_2 is fed from a Parr reactor where it is prepared to be water-wet at the experimental conditions (1550 psi, 40°C).

2.2. Core Characteristics

The porosity and permeability of the Buffi Berea sandstone samples (Fig. 3) have been measured using a CoreTest AP-608 Poro Permeameter. Sample BO5 exhibited a porosity of 24.10%, with an air permeability of 985.15 mD and an absolute permeability of 966.97 mD. Its measured pore volume was 20.36 cc. Sample B03 showed a similar porosity of 23.95%, along with air and absolute permeabilities of 982.81 mD and 955.32 mD, respectively, and a pore volume of 20.10 cc. The high porosity and permeability makes the chosen cores suitable for this investigation of the microbubble injection in a high permeability setting. High permeability Berea

represent the upper range of permeabilities encountered in saline aquifers, where injectivity and near-wellbore effects are expected to be critical for CO_2 storage operations.

2.3. Experiment protocol

Volume balance core floodings have been carried out under different settings which have all been compiled in Table 2. Test numbers are in chronological order. Some numbers are missing as the experiment has been carried out but failed due to a recording or injection issue. Most experiments in this study were conducted at a base flow rate of 0.05 cc/min, matching the conditions used by Zhai et al. (2020) to investigate microbubble flow away from the injection wellbore. In sequential tests, higher flow rates of 0.1 and 0.5 cc/min were subsequently applied to evaluate the flow-rate sensitivity of microbubble injection. Reference floodings at 0.1 and 0.5 cc/min from full water saturated core were realised to compare with the sequential injection protocol in both injection types,

Table 2
Volume balance core flooding experimental tests settings and brine permeability monitoring test indented for both BO5 and BO3 samples. Brine permeability was monitored for the test numbers 20 to 31.

Sample name	Test number	Test type
BO5	2–5, and 13–18	Conventional injection 0.05cc/min only
	6–9 and 12	Microbubble injection 0.05cc/min only
	11	Microbubble injection 0.1cc/min only
	10	Microbubble injection 0.5cc/min only
BO3	19	Conventional injection 0.5cc/min only
	20	Conventional injection 0.1cc/min only
	24–28	Microbubble injection Sequential 0.05 ◊ 0.1 ◊ 0.5 cc/min
	30–31	Conventional injection Sequential 0.05 ◊ 0.1 ◊ 0.5 cc/min

The flow rates used in this study are sufficiently low to maintain a capillary-dominated regime (Ca = 1.15–11.5 × 10^{-9}) and to avoid inertial effects, while remaining high enough to generate a measurable pressure drop across the ~ 1 D cores. The porous-media Bond number is estimated to be 1.3×10^{-7}, which is much smaller than unity and demonstrates that buoyancy forces are negligible at the pore scale. As a result, gravity segregation is not expected during the horizontal core-flood experiments, and the observed displacement behaviour is governed by capillary forces rather than density contrasts. In comparison, the mobility ratio is inherently unfavourable: the brine-to-CO_2 viscosity ratio is 16.6, so within the Buckley–Leverett framework the mobility ratio can be expressed as the ratio of relative permeabilities multiplied by this large factor. This qualitatively highlights the strong tendency for CO_2 to be more mobile than brine, implying that any improvement in sweep efficiency or injectivity must arise from reductions in effective gas mobility (e.g., microbubble effects) rather than from favourable viscous or gravitational stability.

The injected brine is synthetic, prepared from deionised water. The salinity is only contributed by NaCl at 125 g/L (12.5 wt%). This value has been chosen to remain close to previous work on microbubble injection (Jiang et al., 2019; Patmonoaji et al., 2019; Zhai et al., 2020).

For any given flooding setting, the protocol remained similar. The Teflon-jacketed core with a Viton rubber layer was inserted in the core holder. The cell was filled with deionised water with a red colour dye to spot any confining leaks during the flooding. The confining pressure was first set to 750 psi (5.17 MPa). The sample was then put under vacuum for at least 24 hours. The vacuuming process was completed when the pore pressure had dropped to a plateau. Following this, the brine was injected at 5 cc/min until the pore pressure reached 100 psi. Both pore and confinement pressures were then increased at the same rate until the target was reached (pore: 1550 psi (10.7 MPa), confinement: 2175 psi (15 MPa)).

From there, for all sequential floodings, a brine permeability test under flooding pressures was performed after the initial brine imbibition: the inlet and outlet pressure transducers recorded their pressures while three flow rates were applied: 10, 20, and 30 cc/min, with short breaks in between to allow the pressure to drop. The pressure difference (ΔP) was then extracted, and brine permeability was calculated using Darcy's law and sample characteristics.

The CO_2, pre-equilibrated with brine, was fed to the pump with the required amount of CO_2 for the experiment (2 pore volumes were estimated to be sufficient to reach breakthrough and recover all the brine, 45 cc was chosen as a higher boundary estimation). Confinement and injection pumps were heated at 40°C and left for one day for the temperature to equilibrate to the target. Once reached, the CO_2 flooding started, the flowrate was set as an input with the required injection amount, and the scale and pressure transducers were set to record until the flooding ended. The pore pressure rose from 1550 psi to 1580 psi (Back pressure regulator cutoff pressure) and the experiment stayed at this pressure until the flooding ended.

Upon ending, both confinement and pore pressure were let down progressively to 750 psi and zero respectively. The sample was vacuumed again, and another experiment could then be carried out.

For sequential tests, once 45 cc of CO_2 was injected, the new flowrate was set, and 45 more ccs were injected until the three flowrates had been carried out. It should be noted that the core holder was changed for these sequential tests, and dead volume measurements were run again for adjustments.

2.4. Recording

To record the output water volume, a camera was installed in front of the recovery cylinder. Photos were being taken every 1 to 2.3 mins and directly stored in the recording computer under its shoot date and time. The confinement pressure was monitored via its own pressure transducers, both in the pump and in the core holder confinement output. The inlet and outlet pressure were recorded by transducers connected to the recording computer.

2.5. Microbubble generation and injection

Microbubbles were generated using a filter provided by RITE (The Research Institute of Innovative Technology for the Earth) / Tokyo Gas and placed at the sample inlet. In this study, brine is flowing through the filter, then CO_2 follows. With an average pore size of 4 microns, it created bubbles expected to be in the order of tens of micrometres in size.

The filter was also expected to generate an extra pressure drop, caused by both its lower permeability and by fines migration from particles present in the brine. During microbubble tests, these particles could stop at the filter and decrease the overall permeability, likely in a different order of magnitude compared to the core alone. Therefore, quantitative comparison in permeability between conventional and microbubble experiments could not be made. Instead, only the decay rate was compared, as it provided more insights into the impact of microbubble injection on the sample permeability.

2.6. Permeability measurements fit and uncertainties

During repeated CO_2 floodings, the rock sample undergoes multiple mechanisms of alteration, which may lead to permeability decay:

- Fines migration: with a narrow distribution of pore throat sizes ,the case in Berea sandstone, events of clogging lead to exponential decay of open pore throats (Borisova & Adler, 2005).
- Many models of mineral dissolution precipitation are based on exponential laws with asymptotes due to the limited quantity of reactive material and decay in reactive surface (Noiriel, 2015).

To estimate the characteristic decay time τ associated with the permeability decay of samples, a single exponential with asymptote model is applied to both conventional and microbubble injection decay curves measured for the sample BO3. This curve fit is commonly used in the literature to fit permeability decay data (Hall, 2025). The sample BO5 with a before-and-after flooding permeability measurement has undergone a similar decay. The exponential permeability decay curve fit is expressed as follows:

$$k\left(t\right) = k_{\infty} \ + (k_0 - k_{\infty})\exp(-\frac{t}{\tau})$$

Where:

$$K_{\infty} \ : Asymptotic\, permeability \ \left(mD\right)$$

$$K_0 : Fixed\, initial\, permeability$$

$$t : Exposure\, time \ \left(days\right)$$

$$\tau \ : Decay\, time\, constant \ \left(days\right)$$

The global permeability relative uncertainty is up to 6.3%. It is dominated by viscosity as water temperature after flooding may not be consistently up to the desired temperature during the permeability test. It contributes to 80% to the measurement uncertainty). The reading pressures (± 0.1%), flow rates, and sample dimensions barely matter in comparison (less than 2.6% relative uncertainty impact on the measurement).

3. Results

3.1. Replica experiment (0.05 cc/min)

Replication experiments with a similar protocol to Zhai et al. (2020) have been carried out to investigate the microbubble injection potential on high-permeability samples. Microbubble and conventional injection flooding have been carried out the Berea sample BO5. Results are expressed in a violin plot (Fig. 4). The mean steady state CO_2 saturation is higher for microbubble injection by 8.89%. Saturation distributions and their error bars overlap substantially. Conventional flooding results are mostly clustered around 25%, whereas microbubble injection tends to show values closer to 45%.

As per their respective saturation curves, examples of the ΔP variation along with sample CO_2 saturation from effluent collection are displayed in Fig. 5. The CO_2 saturations curves are mostly subdivided in two zones: A sharp almost-linear increase and a plateau with little episodic increases. There are a few differences between injection types ; the saturation gradient seems to be slower in the conventional case. The remarkable detail is a ΔP up to 3 times higher in the microbubble than conventional injection. It is partly due to the presence of the filter, which has a significantly lower permeability than the sample itself.

3.2. Sequential flowrate tests

Sequential tests have been performed on BO3 sample to test microbubble sensitivity to injection rate. Four tests have been carried out for each injection type. They have been compiled in three violin plots to understand their distribution. The first stage, like replication experiments (Fig. 6), shows a clear and drastic distinction of saturations between conventional and microbubble injection. The microbubble saturations are more spread, and in globality always lower than conventional, with a difference of 25.7% CO_2 on average.

In the case of the later stages of sequential injection (Fig. 7). Distributions are in this case clearly more in favour of conventional injection, where microbubble injection's mean saturations are lower by 13.43% and 9.98% for 0.1 and 0.5 cc/min respectively. Microbubble saturation performance at higher flowrates has narrowed the gap with conventional injection, the saturation difference at 0.05 cc/min has partially faded.

The performed reference floodings show the importance of the flooding protocol on saturations. They show an advantage of microbubbles over a large difference (respectively 31.66 and 13.9% for 0.1 and 0.5 cc/min).

3.3. Sequential tests permeability monitoring

Brine Permeability results are shown in Fig. 8. Data from microbubble injection is up to test 28 as the permeability has been recorded but does not evolve from there. They record the permeability evolution of BO3 during its exposure to CO_2 floodings. Curve fitting equally shows a decay rate difference four times higher for microbubble in comparison to conventional.

4. Discussion

4.1. Filter impact on pressure and global permeability

Microbubble floodings are characterized by a significant higher-pressure difference between inlet and outlet. Figure 5 has shown a 3 times higher pressure difference between microbubble and conventional injection. Microbubbles effect on pressure is documented: Their small size or their collection can cause pore plugging (Le et al., 2022; Telmadarreie et al., 2016).

It is important to note that the microbubble experiments employed a filter with permeability far lower than that of the Berea sandstone core. As a result, the pressure drop in the microbubble experiments is dominated by the filter rather than the rock. Therefore, ΔP values between microbubble and conventional injections cannot be directly compared, and the observed higher ΔP in microbubble tests does not reflect primarily microbubble–rock resistance but the hydraulic limitation of the filter. Interpretation of pressure signals must therefore be restricted to within-experiment trends rather than cross-mode comparisons. To allow such comparison, a separated generation device would be required to separate both phenomena.

Both conventional and microbubble injection saturation curves are distinguished by their absence of transition zone. Under capillary-dominated conditions (low capillary number), displacement is controlled by pore-scale capillary entry pressures, leading to sharp invasion fronts and saturation gradients that may be unresolved at the experimental scale (Blunt, 2017).

4.2. Flow Rate–Dependent Performance of Microbubble Injection

Our volume-balance core flooding experiments on high-permeability Berea sandstone (~ 980 mD) reveal a strong dependence of microbubble efficacy on injection flow rate. At the lowest tested rate (0.05 cc/min), microbubble injection increases average CO_2 saturation by 8.89% on average relative to conventional injection, a modest but statistically discernible improvement consistent with prior studies in high-permeability media (Wang et al., 2025b; Zhai et al., 2020). This enhancement is likely due to Jamin effect: microbubbles temporarily block high-permeability pathways, diverting flow into less-swept intermediate pores and improving displacement efficiency.

However, this advantage vanishes at higher flow rates (0.1–0.5 cc/min), where conventional outperforms microbubble injection by 14–10% in final saturation. At these rates, the added hydraulic resistance from the microbubble generation filter (which increases ΔP by up to 4 times; Fig. 5) may exacerbate preferential flow along dominant channels, worsening sweep uniformity. These findings indicate that the benefits from low-flow laboratory studies may not be directly applicable by extrapolation to field-scale injection scenarios, where near-wellbore flow rates are typically much higher, and suggest the need for further research under higher flow rates considering practical operation. Microbubble injection is significantly affecting the flow, for better or worse. The filter permeability is much smaller than the sample permeability, inducing a stronger ΔP, which induces microbubble smaller saturation results.

At the investigated flow rates (0.05–0.5 cc/min), the experiments remain within a capillary-dominated regime. However, in high-permeability samples, the characteristic capillary pressure contrast between large and small pores is small. This reduces the stabilizing effect of capillary forces on the displacement front. Under these conditions, CO_2 invasion becomes highly sensitive to pore-network geometry, connectivity, and experimental layout. Consequently, small differences in sample heterogeneity or injection sequence can lead to markedly different saturation outcomes, as observed between BO3 and BO5.

For the sequential injection protocol, microbubble injection offers worse results than conventional. Whereas floodings from full saturation show the opposite trend. CO_2 microbubbles can be hypothesised as being generated on the first injected volumes, as water is available in the filter's pores. However, It can be inferred that once CO_2 breaks through the filter, the conditions for microbubble generation are no longer met, resulting in few to none being created. This shows the need for CO_2 to be co-injected in the brine to effectively work after filter breakthrough, which has not been done in many publications (Jiang et al., 2019; Park et al., 2018; Patmonoaji et al., 2019; Wang et al., 2022; Xue et al., 2014; Zhai et al., 2020).

4.3 Saturation Variability and Sample History Effects

Saturation distributions show a widespread distribution, going above the expected variance by 3.24% for conventional and 4.28% for microbubble injection on average. Microbubble having a larger variance due to experimental setup, one cannot conclude on a higher variability caused by microbubble injection itself. The permeability monitored sample (BO3) shows a gradual permeability decay which suggests a high pore space alteration due to chemical reactions or other mechanical effects (Fig. 8). The saturation results spread could be caused by several mechanisms in action in these experiments:

- The use of high-permeability samples, where their flow dynamics can be very variable from one flooding to another due to potential channelling effects (Tawiah et al., 2021).
- Progressive geochemical alteration of the core due to repeated CO_2 exposure. Even after brine re-saturation between floods, residual acidic brine and dissolved CO_2 may persist in pore spaces, altering wettability or precipitating secondary minerals (Zhao et al., 2015). Over successive cycles, this can reduce effective porosity and shift capillary pressure curves, leading to inconsistent displacement behaviour.
- Heterogeneity in microbubble generation and transport. The mechanical filter produces a polydisperse bubble population whose size distribution may vary slightly between runs. In high-permeability media, where pore-throat sizes exceed typical microbubble diameters (1–50 μm), minor changes in bubble size or concentration can significantly affect plugging dynamics and sweep pathways.

Overall, these observations highlight the value of repeated-flood laboratory studies in capturing cumulative effects that may not be apparent in single-injection experiments, but which are likely to play an important role during prolonged CO_2 injection under field-scale operating conditions.

4.4 Sample alteration

Brine permeability monitoring shows a different aspect of the multiple flooding cycles dynamic: The decay of the BO3 sample follows a single exponential with asymptote model. When identifying the decay time constant, microbubble injection has a higher value compared to conventional (≈ 4 times higher), showing a potentially higher reactivity and sample decay. Microbubbles have a larger surface area and can dissolve in the brine at a

faster rate (Xue et al., 2011). While dissolution can initially increase porosity, it often leads to pore collapse, fines mobilisation, or clay swelling, ultimately reducing permeability (Bhuvankar et al., 2023; Xu et al., 2004).

On a field scale, prolongated injection can cause injectivity issues due to CO_2-brine rock interactions altering the pore structures to diminish the pore throat radius (Zhao et al., 2015). Critically, this effect is most pronounced in the near-wellbore region, where CO_2 concentration and contact time are highest, which is precisely the zone governing injectivity in field operations. Thus, while microbubble injection may improve storage efficiency in the far field, a potential challenge is the long-term maintenance of well injectivity.

A multiple flooding approach with monitoring of permeability allows for a better estimation of the field expected saturation, as well as its potential to decay in permeability due to the presence of CO_2. Nonchemical microbubble injection is a technique that presents an economical interest in applying it to large scale due to its simple generation and reliance on self-stability.

4.3 Study limitations

This study suffers from several limitations:

- The Buffi Berea sandstone studied here has high permeability which has a few comparison points with current literature on microbubble injection.
- The large gap between variance and absolute uncertainty for CO_2 saturations given for each flowrate makes it difficult to conclude on a definite number.
- The pressure drop between conventional and microbubble injection is not perfectly understood and comparable. The current setup is not able to separate the action of the filter and the microbubble flow on the ΔP.
- The pressure difference curves are influenced by the back pressure regulator behaviour. It creates artifacts, mainly pressure bumps, caused by the difficulty of the regulator to stabilise CO_2-brine flow.
- The data given by low flowrate (0.05cc/min) sequential tests (on sample BO3) does not match previous data on replication floodings (BO5), which can reveal a sample dependency on results.
- The BO3 core experienced several consecutive CO_2 floods, so the observed permeability decay accumulates over time and cannot be attributed uniquely to the injection mode. The fitted decay time constant appears higher during microbubble injection; this should not be taken as a definite proof of enhanced chemical reactivity driven specifically by microbubbles. The microbubble filter may introduce hydraulic resistance or host geochemical alteration, adding uncertainty to the decay trend. The apparent difference in decay rates suggests only a possible tendency rather than a microbubble-specific mechanism. Further tests on fresh cores without filters are necessary to draw mechanistic conclusions.

5. Conclusion

Microbubble CO_2 injection is an emerging injection technique, predominantly investigated through mechanical generation using microporous filters at different injection rate protocols. Conclusions are listed below:

- The replication experiments (0.05cc/min) show disparate results between samples. Microbubble injection is likely to perform better on average, shown by a mean of 37.00% in comparison to 28.11% for conventional on the BO5 sample. However, the BO3 sample shows an opposite trend, where conventional is advantaged

by 25.72% in CO_2 saturation compared to microbubble injection. Overall, many factors such as the high permeability, sample heterogeneity and sample gradual change during experiments might explain these results.

- Higher injection flowrates in sequential injection are globally advantageous to conventional injection. Reference floodings done from complete water saturation (reference floodings) show an opposite trend to sequential injection, where conventional performs less than microbubble. This could be explained by the need of a water phase for microbubbles to be generated. This supports the need for co-injection on the field scale.
- All tests are affected by an important standard deviation in comparison to the expected variance, in particular with microbubble injection (conventional: 3.24%, microbubble: 4.28%). The difference is however not large enough to be conclusive. The optimal flowrate and ratio for microbubble injection are still to be found and optimised.
- The sample BO3 brine permeability has been monitored before every flooding. The permeability has drastically decreased along all the observed floodings from 955.318 mD to 288.2 mD. Single exponential with asymptote fits on separated conventional and microbubble injection data shows a much higher characteristic decay time τ for microbubble injection. A higher permeability decay for microbubble injection warrants further investigation.

Finally, these results support the broader conclusion of the study: while previous work on microbubble CO_2 largely focused on low-permeability formations has shown consistent improvements in sweep and trapping, our experiments demonstrate that in high-permeability systems, MB CO_2 behaviour is strongly rate-dependent and may lead to injectivity difficulties under certain conditions.

Sequential flooding allows us to capture cumulative and rate-sensitive effects, providing realistic insight into potential trade-offs for CCS deployment. While microbubble CO_2 is beneficial in low-rate or far-field regions, it may pose near-wellbore injectivity difficulties. These findings underscored the need for further research under higher flow rates considering practical operation, and emphasising the need for careful rate optimisation, injection design, and long-term integrity assessment.

Declarations

Consent to publish

Not applicable

Consent to Participate

Not applicable

Competing Interests

Theo Le Gallais reports that financial support was provided by Tokyo Gas Australia Pty Ltd. His tuition fees for PhD candidacy have been off-set by Curtin University.The other authors declare that they have no known

competing financial interests or personal relationships that could have appeared to influence the work reported in this paper.

Funding declaration

The research included in this paper was funded by Tokyo Gas Australia Pty Ltd. Curtin University has off-set the tuition fees of PhD candidates involved in the project.

Author Contribution

Theo Le Gallais : Conceptualization, methodology, investigation, data curation, formal analysis, writing - original draftEgi Adrian Pratama: Investigation, formal analysis, writing - review & editingKlaus Regenauer-Lieb, Mohammad Sarmadivaleh : Writing - review & editing, supervisionAli Saeedi: Methodology, supervision, review & editingQuan Xie: Writing - review & editingHideto Kurokawa: Writing - review & editing

Acknowledgement

The authors would like to deeply thank the contribution of Tokyo Gas and RITE for their continuous support and also in providing the microbubble generation filters used in this study.

Data Availability

The data that support the findings of this study are available from the corresponding authors upon reasonable request.

References

1. Aizawa Y, Baba Y, Xue Z. (2021). Microbubble CO2 Injection for Geological Sequestration in Tight Sandstone Reservoirs. *Proceedings of the 15th Greenhouse Gas Control Technologies Conference 15–18 March 2021*. https://ssrn.com/abstract=3811393
2. Bhuvankar P, Cihan A, Birkholzer JT. (2023). Pore-Scale Analysis of the Permeability Damage and Recovery during Cyclic Freshwater and Brine Injection in Porous Media Containing Non-Swelling Clays. Energies, *16*(22).
3. Blunt MJ. Multiphase Flow in Permeable Media: A Pore-Scale Perspective. Cambridge University Press; 2017. https://doi.org/DOI.
4. Borisova EA, Adler PM. Deposition in porous media and clogging on the field scale. Phys Rev E. 2005;71(1):016311. https://doi.org/10.1103/PhysRevE.71.016311.
5. Dubey S, Majumder SK. (2024). Stability analysis of CO2 microbubble for CO2 sequestration and mobility control in enhanced oil recovery. *Chemical Engineering Journal*, *500*. https://doi.org/10.1016/j.cej.2024.156595

6. Hall C. (2025). *Reactive transport in cement-based materials* (Hall's Notes and Queries, Issue. https://blogs.ed.ac.uk/christopherhall/wp-content/uploads/sites/6693/2025/09/NQ11.pdf
7. IEA. (2020). *Energy Technology Perspectives 2020*.
8. IPCC. (2023). Climate Change 2023: Synthesis Report. *IPCC*. https://doi.org/https://dx.doi.org/10.59327/IPCC/AR6-9789291691647.001
9. Jia H, Yu H, Wang S, Shi J, Xie F, Wang S, Lu J, Wang Y, Zhang F. Investigation of CO2 microbubble assisted carbon sequestration and gravity-induced microbubble ripening in low permeability reservoirs. Appl Energy. 2024;373. https://doi.org/10.1016/j.apenergy.2024.123954.
10. Jia H, Yu H, Xie F, Yuan Z, Xu K, Wang Y, RESEARCH ON CO2 MICROBUBBLE DISSOLUTION KINETICS AND ENHANCED OIL RECOVERY MECHANISMS. Chin J Theoretical Appl Mech. 2023;55(3):755–64. https://doi.org/https://doi.org/10.6052/0459-1879-22-507.
11. Jiang L, Xue Z, Park H. Enhancement of CO2 dissolution and sweep efficiency in saline aquifer by micro bubble CO2 injection. Int J Heat Mass Transf. 2019;138:1211–21. https://doi.org/10.1016/j.ijheatmasstransfer.2019.04.139.
12. Le NNH, Sugai Y, Vo-Thanh H, Nguele R, Ssebadduka R, Wei N. Experimental investigation on plugging performance of CO2 microbubbles in porous media. J Petrol Sci Eng. 2022;211. https://doi.org/10.1016/j.petrol.2022.110187.
13. Li S, Wang X, Wang S, Zhang Y, Chen C, Jiang L, Wang L, Liang F, Sun H, Song Y. Optimizing oil recovery with CO2 microbubbles: A study of gas composition. Energy. 2024;302. https://doi.org/10.1016/j.energy.2024.131836.
14. Li X, Peng B, Liu Q, Liu J, Shang L. Micro and nanobubbles technologies as a new horizon for CO2-EOR and CO2 geological storage techniques: A review. Fuel 341. 2023. https://doi.org/10.1016/j.fuel.2023.127661.
15. Li X, Wang Y, Zeng B, Li Y, Tan H, Zandvliet HJW, Zhang X, Lohse D. Entrapment and Dissolution of Microbubbles Inside Microwells. Langmuir. 2018;34(36):10659–67. https://doi.org/10.1021/acs.langmuir.8b02173.
16. Mahjour SK, Faroughi SA. (2023). Risks and uncertainties in carbon capture, transport, and storage projects: A comprehensive review. *Gas Science and Engineering*, *119*. https://doi.org/10.1016/j.jgsce.2023.205117
17. Noiriel C. Resolving Time-dependent Evolution of Pore-Scale Structure, Permeability and Reactivity using X-ray Microtomography. Rev Mineral Geochem. 2015;80(1):247–85. https://doi.org/10.2138/rmg.2015.80.08.
18. Park H, Jiang L, Kiyama T, Xue Z. Experimental Study of Microbubble CO2 Flooding in Heterogeneous Sedimentary Rock. SSRN Electron J. 2018. https://doi.org/10.2139/ssrn.3365701.
19. Patmonoaji A, Zhang Y, Xue Z, Park H, Suekane T. Experimental and numerical simulation of supercritical CO2 microbubble injection into a brine-saturated porous medium. Int J Greenhouse Gas Control. 2019;91. https://doi.org/10.1016/j.ijggc.2019.102830.
20. Rogers PSZ, Pitzer KS. Volumetric Properties of Aqueous Sodium Chloride Solutions. J Phys Chem Ref Data. 1982;11(1):15–81. https://doi.org/10.1063/1.555663.
21. Tawiah P, Wang H, Bryant SL, Dong M, Larter S, Duer J. Effects of temperature and CO2/Brine cycles on CO2 drainage endpoint phase mobility – implications for CO2 injectivity in deep saline aquifers. Int J Greenhouse Gas Control. 2021;112. https://doi.org/10.1016/j.ijggc.2021.103491.

22. Telmadarreie A, Doda A, Trivedi JJ, Kuru E, Choi P. CO2 microbubbles – A potential fluid for enhanced oil recovery: Bulk and porous media studies. J Petrol Sci Eng. 2016;138:160–73. https://doi.org/10.1016/j.petrol.2015.10.035.
23. Ueda R, Nakano M, Xue Z. The efforts for the application of micro bubble technology to CCS and EOR. J Japanese Association Petroleum Technol. 2021;86(2):94–104. https://doi.org/10.3720/japt.86.94.
24. Wang D, Fan J, Xue Z. Hydrodynamic Analysis of CO2 Migration in Heterogeneous Rocks: Conventional and Micro-Bubble CO2 Flooding Experiments and Pore-Scale Numerical Simulations. Water Resour Res. 2022;58(5). https://doi.org/10.1029/2021wr031874.
25. Wang S, Zhang G, Lv P, Wang Z, Jiang L, Zhu L, Song Y. Accelerating CO2 Dissolution Trapping in Deep Saline Aquifers through a Microbubble Injection Strategy. Energy Fuels. 2025b;39:3217–25. https://doi.org/https://doi.org/10.1021/acs.energyfuels.4. c05889?urlappend=%3Fref%3DPDF&jav=VoR&rel=cite-as.
26. Xu T, Apps JA, Pruess K. Numerical simulation of CO2 disposal by mineral trapping in deep aquifers. Appl Geochem. 2004;19(6):917–36. https://doi.org/https://doi.org/10.1016/j.apgeochem.2003.11.003.
27. Xue Z. Field Application of Microbubble CO2 Injection for Enhanced Storage Efficiency in a Tight Sandstone Reservoir. SSRN Electron J. 2021. https://doi.org/10.2139/ssrn.3811983.
28. Xue Z, Matsuoka T. Lessons from the First Japanese Pilot Project on Saline Aquifer CO2 Storage. Chigaku Zasshi (Jounal Geography). 2008;117(4):734–52. https://doi.org/10.5026/jgeography.117.734.
29. Xue Z, Nishio S, Hagiwara N, Matsuoka T. Microbubble Carbon Dioxide Injection for Enhanced Dissolution in Geological Sequestration and Improved Oil Recovery. Energy Procedia. 2014;63:7939–46. https://doi.org/10.1016/j.egypro.2014.11.828.
30. Xue Z, Park H, Ueda R, Nakano M, Nishii T, Inagaki S. Microbubble CO2 Injection for Enhanced Oil Recovery and Geological Sequestration in Heterogeneous and Low Permeability Reservoirs. SSRN Electron J. 2018. https://doi.org/10.2139/ssrn.3366428.
31. Xue Z, Tsuji S, Kameyama H, Nishio S, Matsuoka T. Development of Carbon Dioxide Microbubble Sequestration into Saline Aquifer and CO2-EOR Reservoirs. Energy Procedia. 2013;37:4628–34. https://doi.org/https://doi.org/10.1016/j.egypro.2013.06.371.
32. Xue Z, Yamada T, Matsuoka T, Kameyama H, Nishio S. Carbon dioxide microbubble injection–Enhanced dissolution in geological sequestration. Energy Procedia. 2011;4:4307–13. https://doi.org/10.1016/j.egypro.2011.02.381.
33. Yu Y, Beddoe C, Xue Z, Chakhmakhchev A, Hamling J, Smith S, Kurz B. (2022). Experimental evaluation of enhanced tight oil recovery performance by microbubble CO2 and microbubble rich gas in North Dakota plays. *Unconventional Resources Technology Conference, 20–22 June 2022*. https://doi.org/https://doi.org/10.15530/urtec-2022-3694645
34. Zhai H, Xue Z, Park H, Aizawa Y, Baba Y, Zhang Y. Migration characteristics of supercritical CO2 microbubble flow in the Berea sandstone revealed by voxel-based X-ray computed tomography imaging analysis. J Nat Gas Sci Eng. 2020;77. https://doi.org/10.1016/j.jngse.2020.103233.
35. Zhang H, Arif M. Residual trapping capacity of subsurface systems for geological storage of CO2: Measurement techniques, meta-analysis of influencing factors, and future outlook. Earth Sci Rev. 2024;252. https://doi.org/10.1016/j.earscirev.2024.104764.

36. Zhao DF, Liao XW, Yin DD. An experimental study for the effect of CO2-brine-rock interaction on reservoir physical properties. J Energy Inst. 2015;88(1):27–35. https://doi.org/10.1016/j.joei.2014.05.001.

Figures

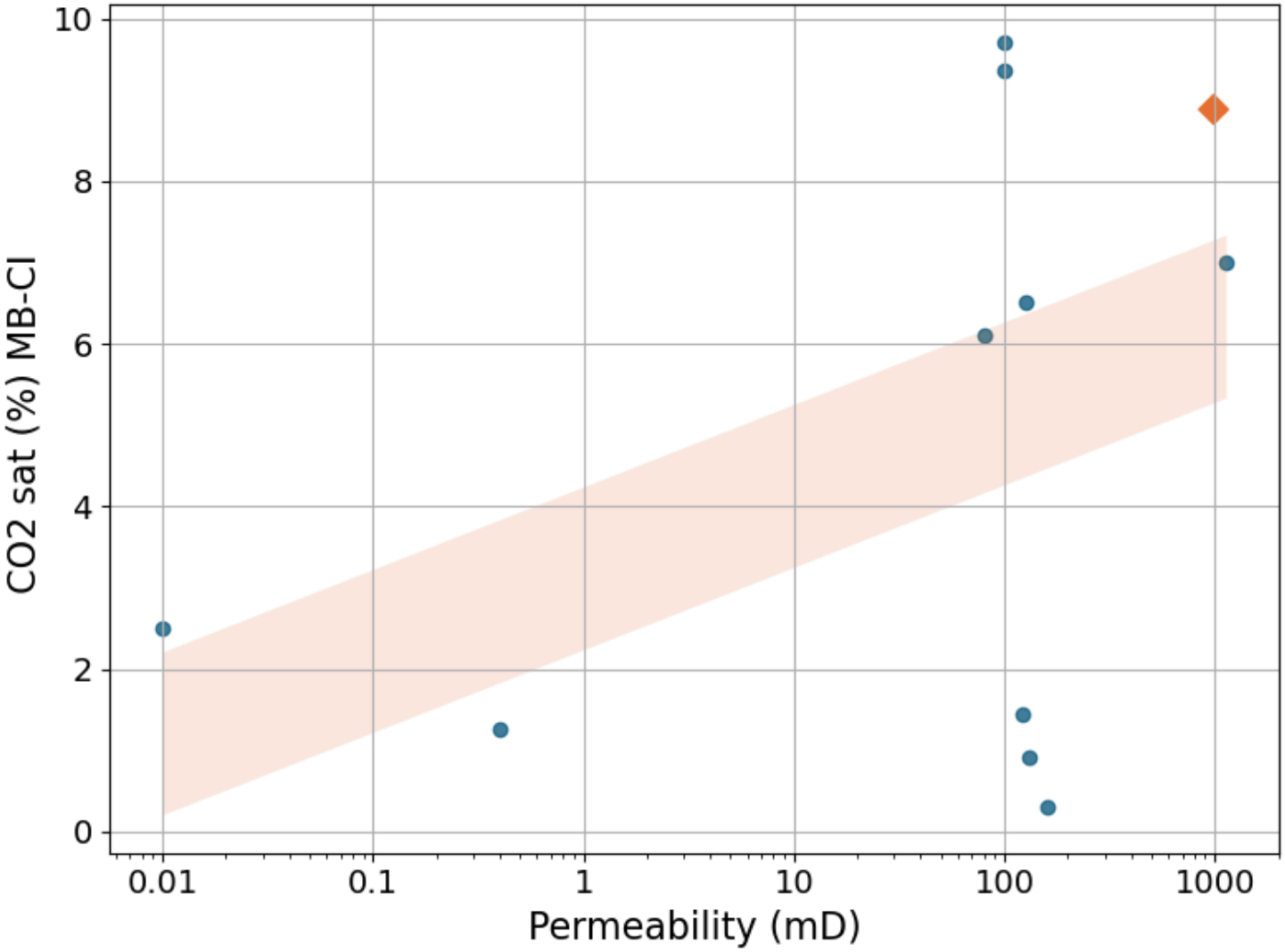


Figure 1

Mean post flood steady state saturation difference (microbubble saturation improvement) over studied sample permeability observed among current flooding studies of microbubble CO_2 injection on sandstone samples in the literature. Triangles: Literature. Diamond: This study. Literature references used : Aizawa et al. (2021); Jia et al. (2024); Jiang et al. (2019); Park et al. (2018); Patmonoaji et al. (2019); Wang et al. (2022); Wang et al. (2025b); Xue et al. (2014); Xue et al. (2018); Xue et al. (2013); Zhai et al. (2020). Xue et al. (2014) and Xue et al. (2013). Aizawa et al. (2021) reports a difference between microbubble and conventional injection to be within 5%, which has been assumed in favour of microbubbles and overall, 2.5% displayed on the graph. The shaded region highlights the trend of greater MB efficacy in high-permeability media.

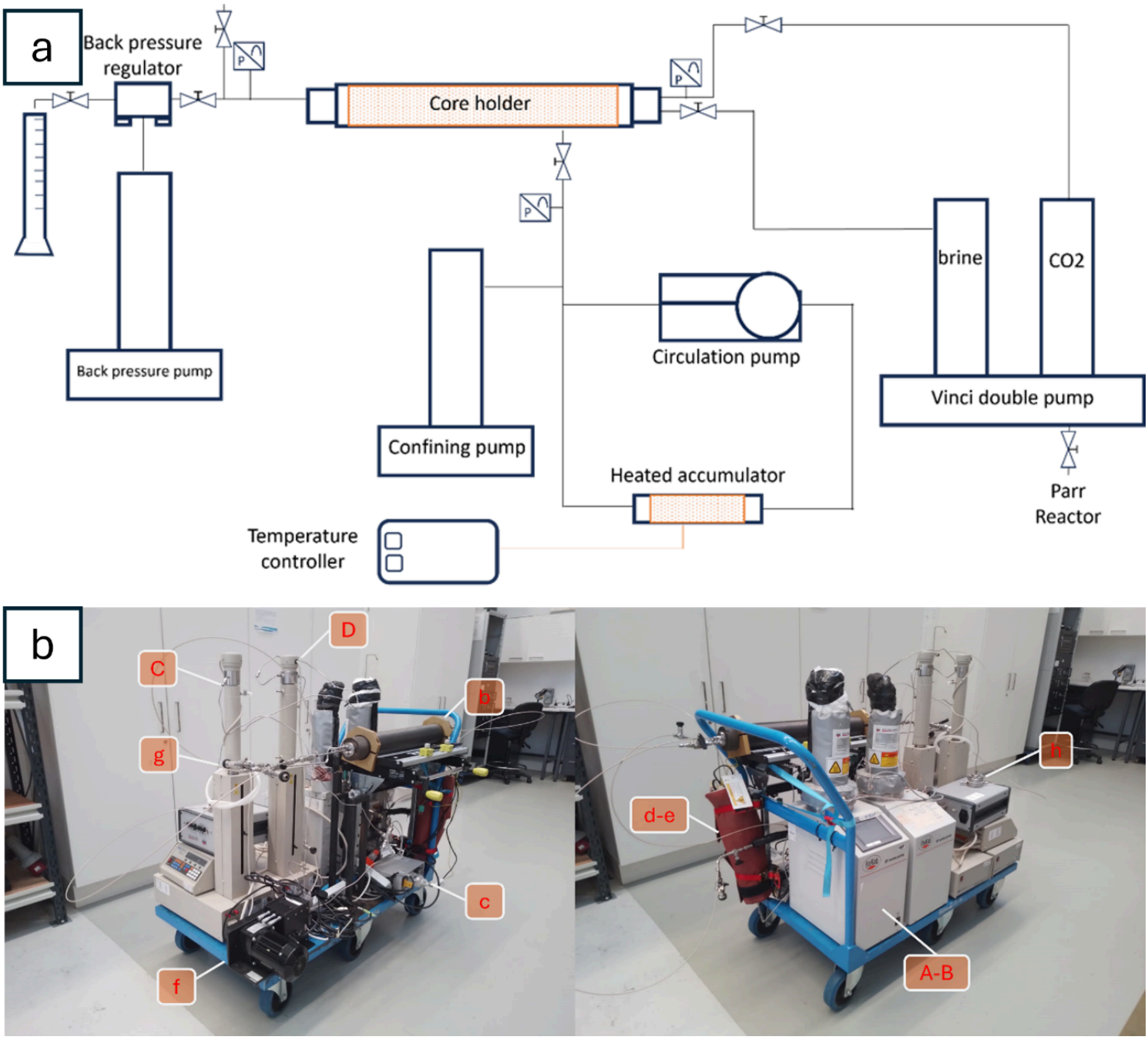


Figure 2

Volume balance core flooding setup. a) Setup diagram. b) Setup photo: A-B) Vinci double pump. C) Confining pressure pump. D) Back pressure pump. d-e) Accumulator and heating tape. f) Circulation pump. g)pressure transducer (back pressure showed). h) Back pressure regulator.



Figure 3

High-permeability Berea sandstone core samples photo. a) BO3. b)BO5.

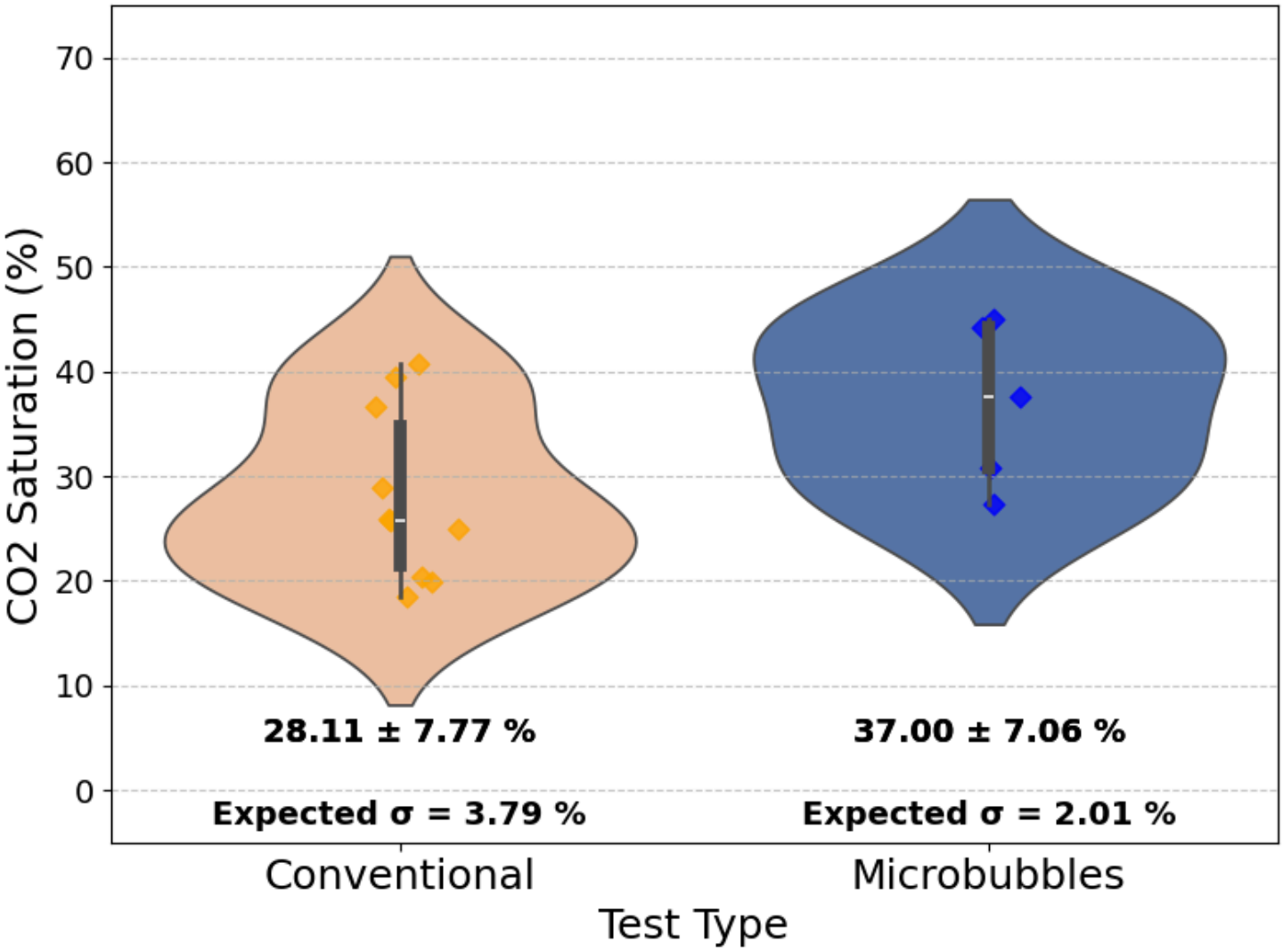


Figure 4

Violin plots of CO_2 saturation results from replica experiments of Zhai et al. (2020)protocol (0.05cc/min) based on 5 floodings for each injection type. The mean, standard deviation and expected variance of each dataset is in black. Diamonds: data points. White line: median. Microbubble yields an average saturation 8.89% higher than conventional.

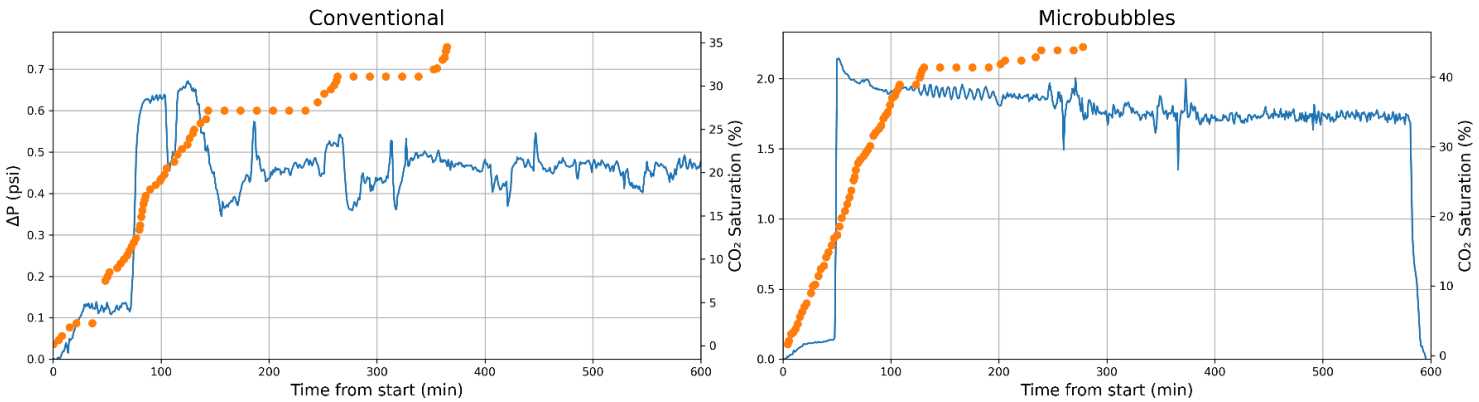


Figure 5

ΔP and saturation curve examples in the volume balance core flooding replicas of Zhai et al. (2020). Orange dots: CO_2 saturation (%). Blue curve: Sample pressure difference (psi). Test no 5 is showing conventional injection trend. Test 7 is showing microbubbles injection trend.

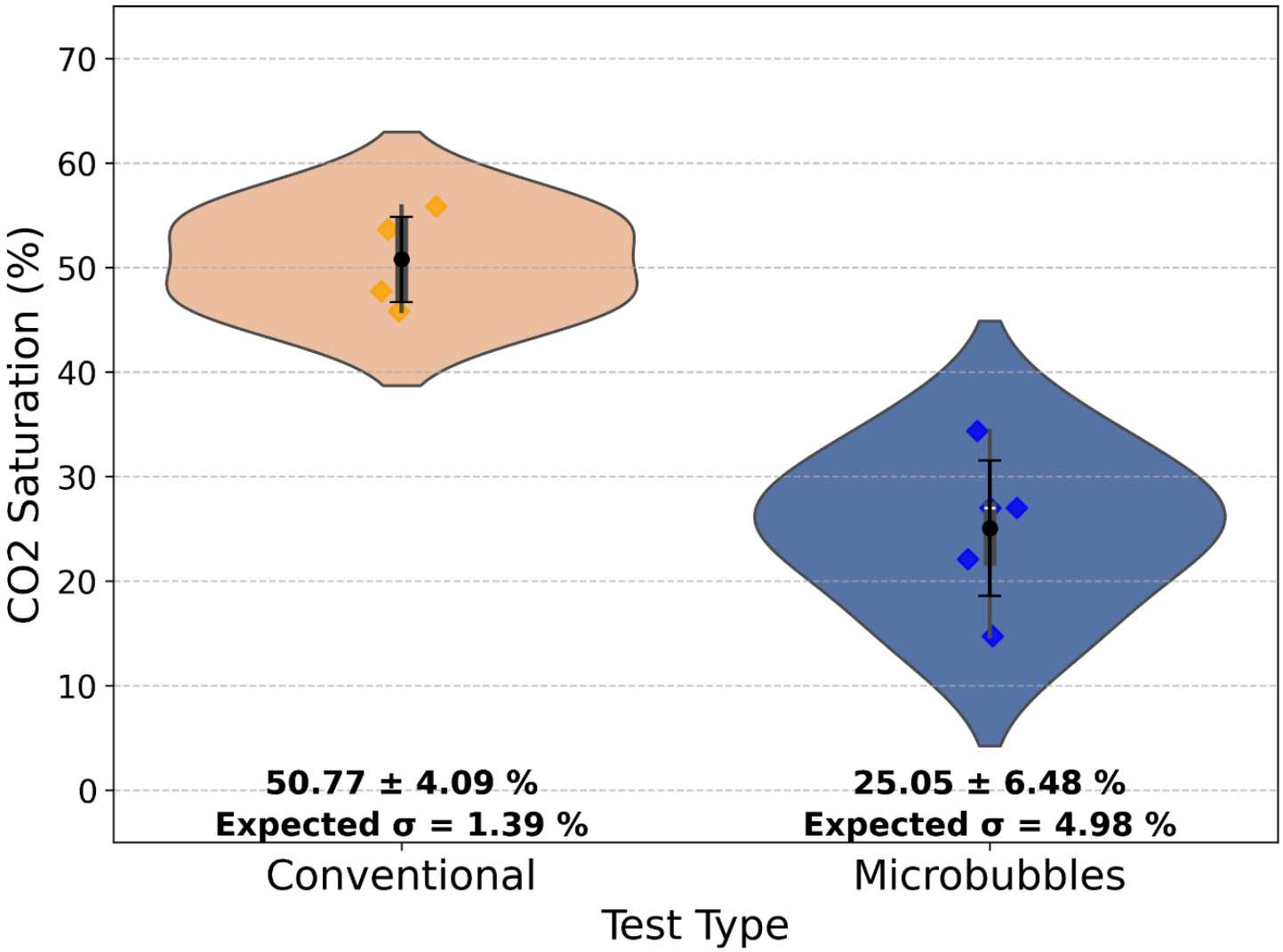


Figure 6

Violin plots of CO_2 saturation results for the BO3 sample from the first stage of sequential injection (0.05cc/min). The mean, standard deviation and expected variance of each dataset is in black. Diamonds: data points.

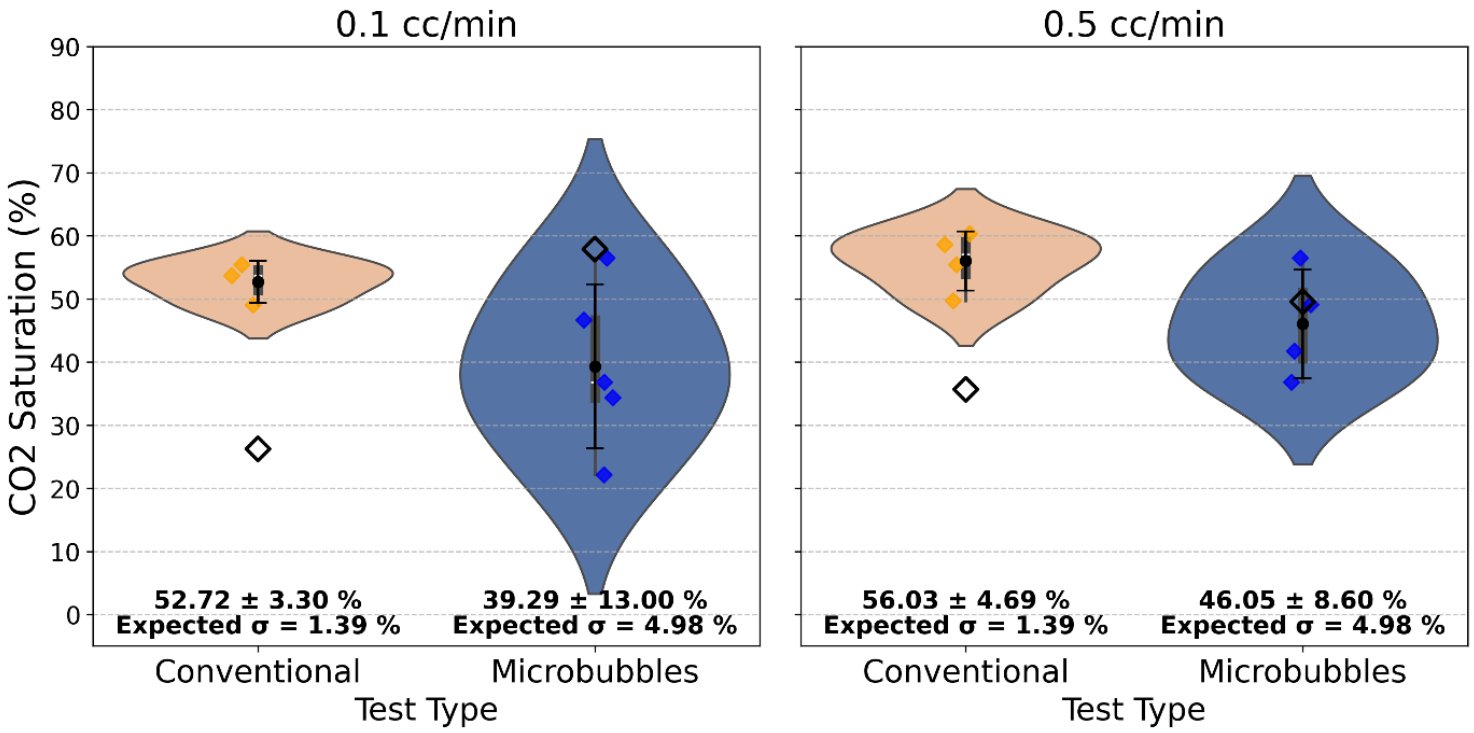


Figure 7

Violin plot of CO_2 saturation results at 0.1 and 0.5 cc/min CO_2 for conventional and microbubble injection. The mean, standard deviation and expected variance of each dataset is in black. Black hollow diamonds: Reference floodings from zero. Blue and orange diamonds: data points.

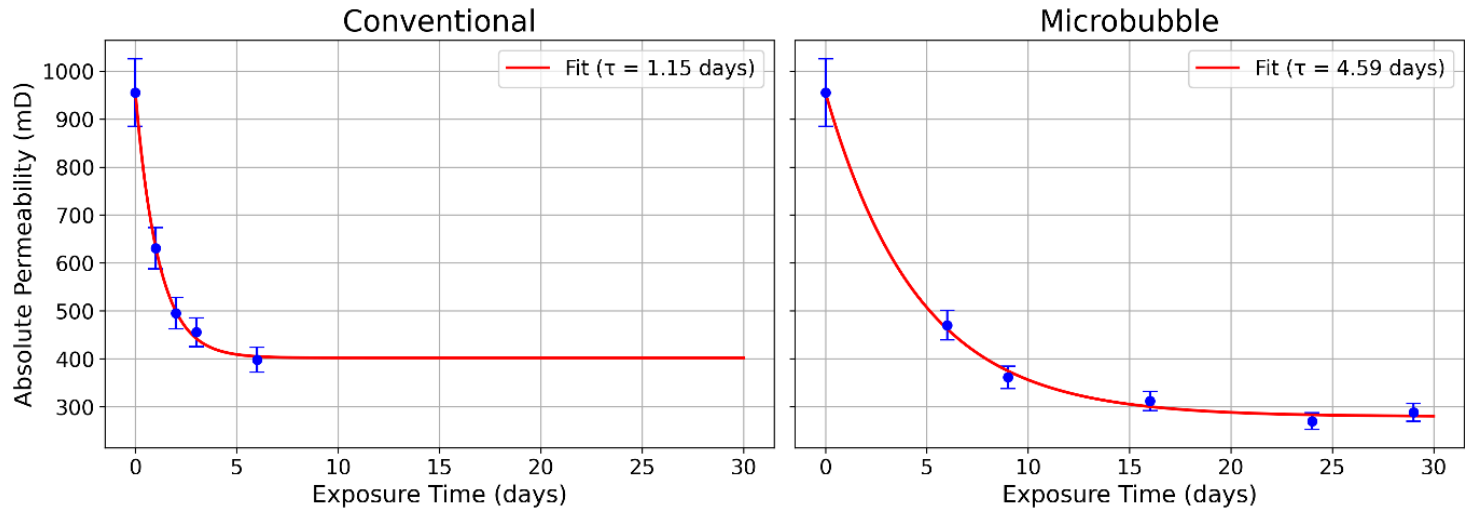


Figure 8

Evolution of brine permeability in Berea sample B03 over sequential CO_2 floods. Microbubble injection causes a fourfold faster permeability decline than conventional injection, fitted with a single exponential with asymptote model.